

Corrosion Inhibition of Mild Steel in Acidic Medium by Magnetite Myrrh Nanocomposite

Ayman M. Atta^{1,2,*}, Gamal A. El-Mahdy^{1,3}, Hamad A. Al-Lohedan¹ and Sami A. Al-Hussain^{1,3}

¹ Surfactants research chair, Department of Chemistry, College of Science, King Saud University, Riyadh 11451, Kingdom of Saudi Arabia.

² Egyptian Petroleum Research Institute, 1 Ahmad Elzomor St., Nasr city, Cairo, Egypt.

³ Chemistry Department, Faculty of Science, Helwan University, Helwan, Egypt.

⁴ Faculty of science, Department of Chemistry, Al-Imam Muhammad Bin Saud Islamic University, Riyadh 11632, Kingdom of Saudi Arabia.

*E-mail: khaled_00atta@yahoo.com

Received: 27 August 2014 / Accepted: 25 October 2014 / Published: 28 October 2014

The development of nontoxic effective corrosion inhibitors for metallic substrates is an issue of great importance for protection of metal alloys and components. Surface properties of new stabilized magnetic nanoparticle (MNP) colloids coated with Myrrh gum were investigated. The natural product Myrrh gum was used as capping agent to produce highly dispersed coated magnetite nanoparticles. The structure and morphology of the magnetic nanogel were characterized by transmission electron microscopy (TEM), X-ray diffraction (XRD) and ultrasizer. Drop shape analyzer was used to examine the surface properties of the produced magnetite nanoparticles. The corrosion inhibition efficiencies of aqueous solutions of Myrrh and Myrrh capped magnetite for steel in 1M HCl solution have been investigated at different concentrations of the inhibitor using potentiodynamic polarization and electrochemical impedance spectroscopy measurements. The results showed that corrosion resistance increased by increasing the inhibitor concentration and inhibition efficiencies up to 91% can be obtained. Polarization curves revealed that this compound acts as mixed type inhibitor. The inhibition efficiency calculated from these techniques are in reasonably good agreement.

Keywords: Magnetite nanoparticle, Myrrh gum; nanocomposite; electrochemical; corrosion inhibition.

1. INTRODUCTION

Combating metal corrosion in acid medium is a serious environmental problem in the oil, fertilizer, metallurgical and other industries. Organic compounds are effective inhibitors of aqueous corrosion of many metals and alloys. Many chemical substances are used to protect metals and alloys

against corrosion. The widely used corrosion inhibitors are organic or inorganic chemicals, expensive and toxic to environment. For proper selection of inhibitors, mechanistic information on corrosion and inhibition processes is needed. As a result, scientists are designing new green inhibitors based on natural products and eco-friendly environmental bio-polymers. The natural products based on the plant origin contain several organic derivatives (e.g. alkaloids, polysaccharides, pigments, organic and amino acids, which can be used as corrosion inhibitors [1-3]. Some of polysaccharides, including gums, have been used as corrosion inhibitors for metals in acidic, alkaline, as well as in saline environments [4,5]. The Literature reveals that a wide range of natural products have been successfully investigated as potential inhibitors for the corrosion of metals in aggressive media [2-5]. The inhibitive mechanism was referred to the adsorption of molecules of phytochemicals of plant extracts on the metal surfaces to block the metal surfaces to prevent the corrosion process [4–6]. It was reported that the yield and the corrosion inhibition activity of the plant extract vary widely and depending on the part of the plant which extracted from the plant [7]. Srivatsava [8] reported that black pepper, tobacco, acacia gum, castor oil seeds, and lignin can be used as corrosion inhibitors for steel in acid medium. Gums, such as Gum Arabic, were used as corrosion inhibitors for metals in alkaline and acidic media [9]. The inhibition was attributed to the presence of oligosaccharides, polysaccharides, arabinogalactan, and glucoproteins (contain oxygen and nitrogen atoms) which are the centers of adsorption to metal surfaces.

Magnetite Fe_3O_4 exhibits unique physical properties like high magnetic characteristics, relatively high conductivity and high ratio of spin polarization [10]. Magnetite is also known as a stable, common and biocompatible mineral of very low toxicity [10]. It is one of the best and most preferred materials to combine with various polymers [11-13]. Nanostructured magnetite has high ability to form nanopolymers when compared to those of the bulk material. These materials are characterized by having a large surface area, a very low density, and also a strong magnetic response. However, the use of these nanostructured materials has some limitations arising from the tendency to aggregate because of their high specific area and strong interparticle interactions [14]. To overcome this drawback, different strategies for the chemical stabilization of the magnetite have been investigated, including the incorporation of polymer structures on the magnetite surface or the functionalization of the magnetite surface [15, 16]. The synthesis methods of iron oxide are based on co-precipitation [17], hydrothermal [18] as well as via high temperature methods [19]. However, the wider use of iron oxide based magnetic nanoparticles is still impeded due to low yield, problems in achieving small, uniform and highly dispersed nanoparticles. So the desired method of synthesis needs a simpler, economical as well as a low temperature process for their enhanced applications. In continuation of our quest for developing corrosion inhibitors with high effectiveness and efficiency, the present work aims to prepare new coated magnetite nanoparticle to use as corrosion inhibitor. Henceforth, we present a high yield, room temperature, one pot and water based new synthetic protocol that yields iron oxide nanoparticles. Moreover, the new capping materials is Myrrh gum a cheap, common and nontoxic natural biomaterials. The aim of this work is thus to yield information of the effect of Myrrh gum capping on the surface properties of Fe_3O_4 nanoparticles. Further, the application of the Myrrh capped magnetite as corrosion inhibitors for steel in the acidic medium will be investigated through electrochemical measurements in 1 M HCl.

2. EXPERIMENTAL

2.1. Materials

Anhydrous ferric chloride, potassium iodide, and ammonium hydroxide (25%) were purchased from Aldrich Chemical Co. and used as reagent for preparation of magnetite. Myrrh gum is a commercial natural product extracted from tree with yellowish red color. The soluble fraction of Myrrh was extracted from ethanol/water (1:1 volume %) and used as capping agents after recovery using vacuum evaporator. The aggressive solutions 1 M HCl were prepared by dilution of analytical grade 37% with distilled water. Steel specimens with chemical composition (wt.%): 0.14% C, 0.57% Mn, 0.21% P, 0.15% S, 0.37% Si, 0.06% V, 0.03% Ni, 0.03% Cr and the remaining iron were used for the measurement of electrochemical studies. The surface preparation of the specimens was carried out using emery paper grade 220, 400, 600, 800, and 1200 and 2000. They were washed with bi-distilled water, degreased ultrasonically in ethanol, and finally dried at room temperature before being immersed in the aggressive solutions.

2.2. Preparation of Magnetite Capped with Myrrh

The procedure for preparation of magnetite capped with Myrrh was prepared as following procedure [20]: 40 g of anhydrous FeCl_3 was dissolved in 300 ml of distilled water to prepare an aqueous solution A. Further, 13.2 g (0.08 mol) of potassium iodide was dissolved in 50 ml of distilled water to prepare an aqueous solution B. The aqueous solutions A and B were then mixed together at room temperature and stirred and allowed to reach equilibrium for one hour while bubbling with pure N_2 to keep oxygen free throughout the preparation procedure. Myrrh (10 g) was solubilized in 100 ml of ethanol: water solvent (1:1 vol %) and added dropwise to the reaction mixture at the same time with 200 ml of 25% ammonia solution at temperature 40°C . The reaction mixture was stirred and bubbled with pure N_2 to keep oxygen free throughout the preparation procedure. Mixing was continued until complete precipitation of black magnetite was achieved. The reaction was continued at the reaction temperature with stirring for 4 hrs. The final product was washed with ethanol and air dried to get the reaction yield percentage of 99.5 %. The same reaction was repeated without Myrrh to prepare uncapped iron oxide nanoparticles.

2.3. Characterization of nanoparticles

Transmission electron microscopy (TEM) micrographs were taken with a JEOL JEM-2100F (JEOL, Tokyo, Japan). A few drops of magnetite nanoparticle solution were diluted into 1 mL of ethanol, and the resulting ethanol solution was placed onto a carbon coated copper grid and allowed to evaporate. HR-TEM images of the nanocomposites were recorded using a JEM-2100F (JEOL) at an acceleration voltage of 200 kV.

X-ray powder diffraction (XRD) patterns were recorded using a D/max 2550 V X-ray diffractometer (X'Pert, Philips, Eindhoven, The Netherlands).

The Ultrasizer ultrasonic spectrometer (Malvern Instruments, Worcestershire, U.K.) can measure sound attenuation and sound velocity as a function of frequency, giving particle size distributions of magnetite suspensions.

The surface tension measurement was measured at 25 °C by means of the pendant drop technique using a drop shape analyzer model DSA-100 (Kruss, Germany). Pendant drops were formed on the tip of a Teflon capillary.

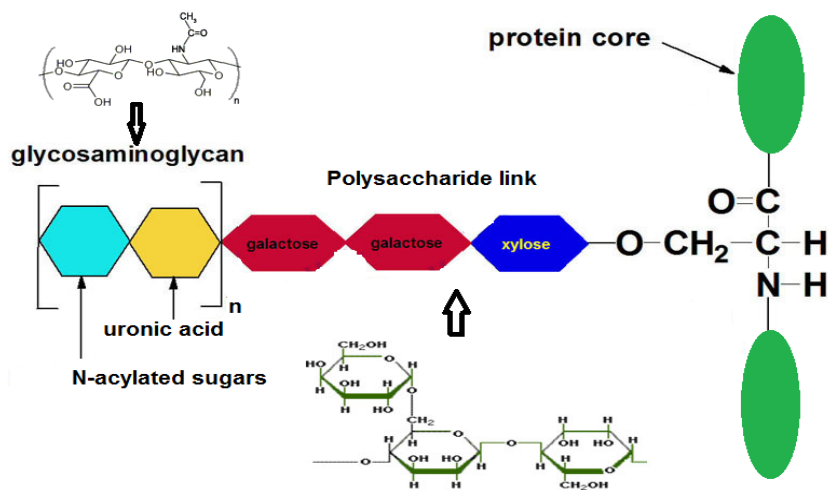
2.4. Electrochemical measurements

Electrochemical measurements were conducted in a jacketed conventional three electrode Pyrex cell. A saturated calomel electrode (SCE) and a platinum electrode were used as the reference and the counter electrodes, respectively. Potentiodynamic polarization measurements were performed using an instrument potentiostat (Solartron 1470E system) with Solartron 1455A as frequency response analyzer to perform all polarization and EIS measurements. The potential scan rate was 5mVs⁻¹. The impedance measurements were carried out in the frequency range of 10 KHz to 10 mHz with a signal amplitude perturbation of 10 mV. Data were collected and analyzed using CorrView, Corr- Ware, Zplot and ZView software.

3. RESULTS AND DISCUSSION

3.1. Characterization of magnetite/Myrrh nanocomposite

Iron oxide particles are bio-compatible and suitable for functionalization with a natural polymer contained amine, carboxylic, aldehyde and hydroxyl functional groups. The surface active molecules can improve the magnetic nanoparticle stability in aqueous solutions by providing steric stabilization [21-24]. The present work reported the effect of Myrrh gum on the surface properties of iron oxide nanoparticles. Myrrh consists of water-soluble gum, alcohol-soluble resins and volatile oil. The gum contains polysaccharides and proteins, while the volatile oil is composed of steroids, sterols and terpenes. Myrrh's characteristic odor is derived from furanosesquiterpenes [25]. Myrrh is partly soluble in ethanol (~ 30 % alcohol soluble material) and is also partly soluble in water and in ether. Since antiquity myrrh has served as a constituent of incense. Myrrh is composed of the essential oil (2–10 %), the ethanol soluble resin (25–40 %) and the water soluble gum (30–60 %). The water soluble gum fraction of myrrh has been found to comprise of a mixture of proteoglycans (with dominating amounts of uronic acid polymers) [25]. The raw gums were heterodisperse systems and contained ~ 70% 4-methyl-glucuronogalactone protein as represented in scheme 1. The main constituents of myrrh was D-galactose, L-arabinose, and 4-methyl D-glucuronic acid (in proportions 4 : 1 : 3) as component of gum myrrh [25].



Scheme 1. Proposed chemical structure of Myrrh.

In the previous work [20] we reported the best conditions to prepare magnetite nanoparticles coated with Myrrh. It was found that the functionalization and dispersability of the magnetite nanoparticles increased in the presence of Myrrh and iodine which produced from reaction between potassium iodide and ferric chloride. Moreover the particle size of magnetite nanoparticles was reduced due to surface modification of magnetite due to presence of iodine [26]. It would be possible to absorb another layer of Myrrh by physical adsorption. It is expected that the formation of covalent bonds between magnetite and Myrrh will be produced from the reaction between the hydroxyls of bare magnetite with the carboxylic, and hydroxyl groups of myrrh. It can be concluded that the prepared magnetite nanoparticle is stabilized via electrostatic attraction between carboxylate groups of myrrh gum and surface hydroxyl groups of Fe_3O_4 which is due to the glycoprotein present in gum [20].

The present work aims to study the effect of Myrrh on the morphology and surface properties of magnetite nanoparticles. In this respect, the XRD was used to confirm the formation of magnetite nanoparticles individually without formation of any iron oxides. The XRD data were represented in Figure 1. The XRD- diffractogram of iron oxide prepared in absence of Myrrh (**figure 1a**) showed the presence of both α and γ phases of Fe_2O_3 contaminated with magnetite. The data showed single peak for tetrahedral coordinated iron of magnetite (Fe_3O_4), and maghemite ($\gamma\text{-Fe}_2\text{O}_3$; whereas octahedrally coordinated iron of hematite ($\alpha\text{-Fe}_2\text{O}_3$) and the two oxyhydroxides, lepidocrocite ($\gamma\text{-FeOOH}$) and goethite ($\alpha\text{-FeOOH}$) showed a split peak. The data proved that the α -phase of iron oxide nanoparticles ($\alpha\text{-Fe}_2\text{O}_3$, hematite) can be formed during the preparation process. This data indicated that the presence of iodine during the formation of magnetite leads to form hematite and maghemite and the formation of hydroxyl groups on the surface of the iron oxide surfaces [20]. Careful inspection of data illustrated in Figure 1b indicates that only magnetite was formed during the capping of magnetite with myrrh in the presence or absence of iodine. These data indicated that the capping agent forms stable layers and prevents the transformation of magnetite into other iron oxides.

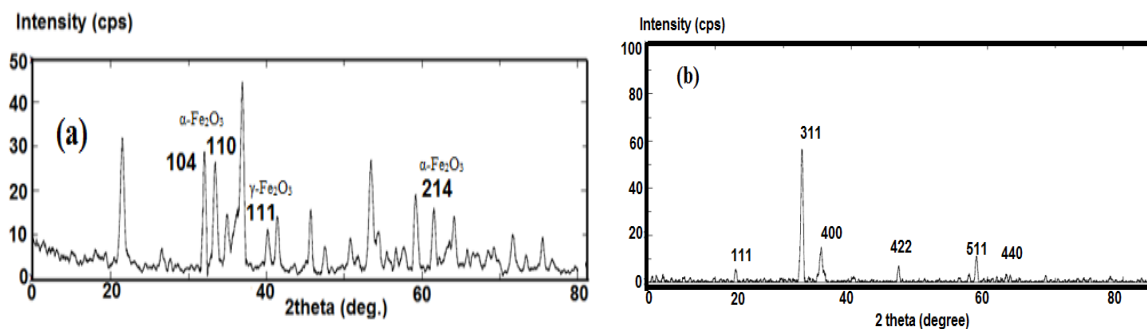


Figure 1. XRD diffractograms of a) iron oxides and b) magnetite/Myrrh nanocomposite.

The encapsulation of magnetite nanoparticles into the Myrrh to form nanocomposite is more interesting and can be represented from TEM (Figure 2). The data revealed that the colloidal stability and distribution increased in the presence of Myrrh and iodine with respect to bare Fe₃O₄ nanoparticles. It is clearly observed that, agglomeration of nanoparticles occur to some extent in the absence of Myrrh gum (figure 2a). Whatever, the colloidal stability of magnetite nanoparticles increases due to successful stabilization of Fe₃O₄ nanoparticles. The repulsion between π electrons of double bonds and carboxylate group of Myrrh prevents full aggregation of nanoparticles [20]. The magnetite/Myrrh nanocomposite is spherical in shape and the Myrrh shell became invisible, the core magnetite particles absorb the electron beam and appear as dark spots within the sphere. TEM images give a feeling for the somewhat monodispersity of the spheres, showing a diameter range of 17–20 nm (Figure 2). The TEM image confirms the presence of core-shell morphology for magnetite-Myrrh; also there is no magnetite leaking outside the Myrrh sphere. The increment of the magnetite/Myrrh nanocomposite size can be referred to the formation of some magnetite aggregates inside the Myrrh shell due to the amphiphilic nature of Myrrh.

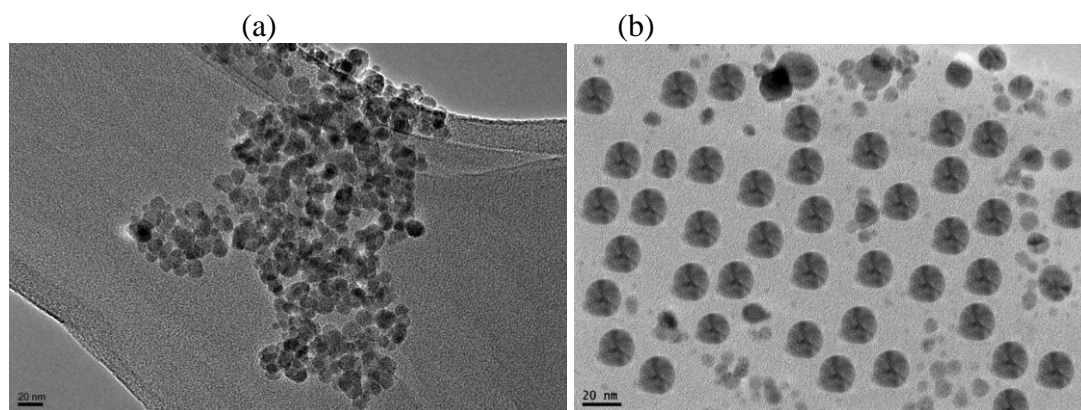


Figure 2. TEM micrograph of a) iron oxide and b) magnetite/Myrrh nanocomposite.

The dispersability and particle size distribution of magnetite/Myrrh nanocomposite can be determined from particle size measurements using Ultrazizer ultrasonic spectrometer (Figure 3). The diameter of the iron oxide nanoparticles in the presence of iodine and absence of Myrrh (figure 2a) was polydisperse between 1 and 10 nm. Ultrazizer measurements of capped magnetite nanoparticle in the

presence of iodine and Myrrh yielded a particle size of 15- 18 nm for Fe₃O₄. The data revealed that the magnetite/Myrrh nanocomposite is highly monodisperse in aqueous media. This nanocomposite can also form a stable dispersion in water and the particle size ranged from 15 to 18 nm which it is similar to TEM measurements.

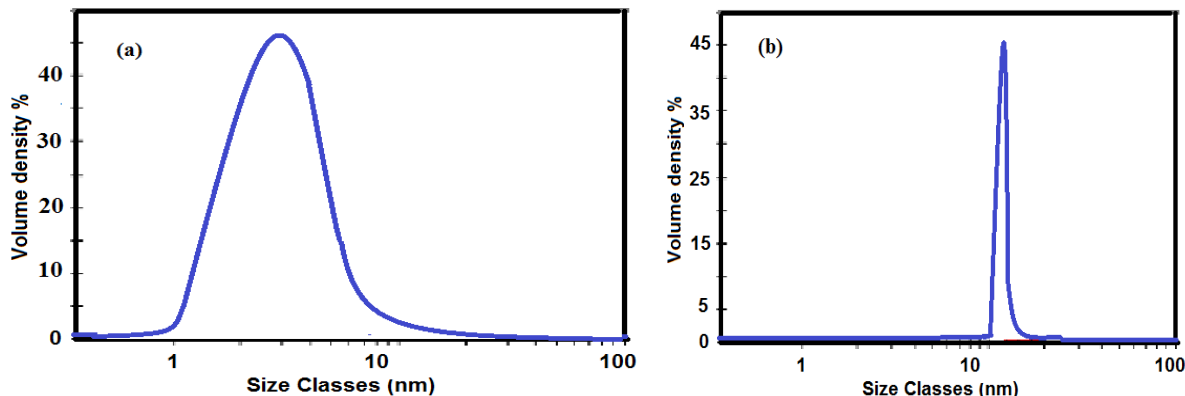


Figure 3. Particle size distribution of magnetite/Myrrh nanocomposite.

Although the surface and interfacial properties are very important for application of nanogels and microgels in dispersions, not too many publications are dealing with this topic, due to the complexity of describing interfacial and surface properties. The literature survey indicated that there is a little information about the surface activity of the dispersed nanoparticles. In the previous works [27-29], we succeeded to prepare surface active nanoparticles. In the present work, the dynamic surface tension of the magnetite/Myrrh nanocomposite was investigated at water/air interface by variation nanocomposite concentrations at 25 °C. The relation between the surface tension and time at different magnetite/Myrrh nanocomposite concentrations were represented in Figure 4. The data illustrated in figure 4 indicated the nanocomposites reached the equilibrium after different time intervals when the concentration lowered from 250 ppm to 50 ppm. The surface tension of water were reduced from 72 mN/m to 43, 51 and 56 mN/m at nanocomposite concentrations. Furthermore, the data represented in Figure 4 indicated that the magnetite/Myrrh nanoparticles reached the surface tension equilibrium with short time with increment their concentrations from 50 to 250 ppm. These data proved that the prepared magnetite/Myrrh nanocomposite highly adsorbed at air/water interface at concentration of 250 ppm.

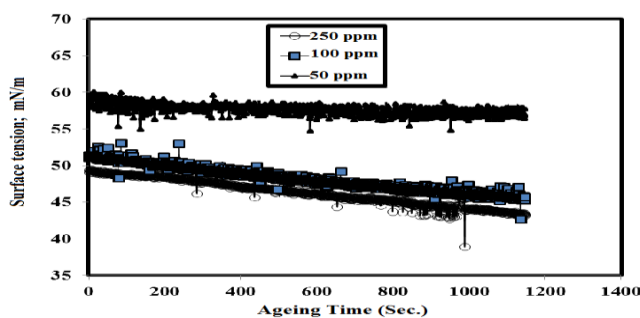


Figure 4. Relation between surface tension and ageing time of magnetite/Myrrh nanocomposite dispersed solutions.

3.2. Polarization measurements

Polarization curves for steel in 1M HCl solution in the absence and presence of Myrrh and Magnetite Myrrh Nanocomposite are shown in Figures 5 and 6, respectively. It is clear that the addition of Myrrh and Magnetite Myrrh Nanocomposite induces a decrease in both anodic and cathodic currents and the cathodic decrease being more significant than in the anodic curve. Hence, the Myrrh and Fe₃O₄ influenced cathodic reaction more than anodic reaction and controls the cathodic reaction more effectively than the anodic dissolution process. The corrosion potential (*E*_{corr}) was observed to shift towards more negative potentials with increasing additive concentration, indicating the inhibitors to be of cathodic character. Corrosion parameters, for Magnetite Myrrh Nanocomposite such as corrosion potential (*E*_{corr}), cathodic and anodic Tafel slopes (*b*_a and *b*_c) and corrosion current density (*i*_{corr}) obtained by extrapolation of the Tafel are listed in Table 1 and 2, respectively. Thus the presence of Myrrh and Magnetite Myrrh Nanocomposite in solution inhibits both the cathodic reactions and the anodic dissolution processes with overall shift of *E*_{corr} to more negative values with respect to the blank solution.

Table 1. Inhibition efficiency values for steel in 1M HCl with different concentrations of Myrrh calculated by Polarization and EIS methods.

	Polarization Method					EIS Method		
	<i>B</i> _a (mV)	<i>B</i> _c (mV)	<i>E</i> _{corr} (V)	<i>i</i> _{corr} μA/cm ²	<i>IE</i> %	<i>R</i> _{ct} Ohm	<i>C</i> _{dl} (μF/cm ²)	<i>IE</i> %
Blank	147.00	141.0 0	-0.4034	745	_____	1.80	334	_____
50 ppm	98.43	96.75	-0.4330	462	37.98	2.9	270	37.93
150	86.93	85.20	-0.4379	268	64.02	5.2	207	65.38
250	106.44	87.02	-0.4671	136	81.74	10.1	136	82.17

Table 2. Inhibition efficiency values for steel in 1M HCl with different concentrations of Myrrh + magnetite nanoparticles calculated by Polarization and EIS methods.

	Polarization Method					EIS Method		
	<i>B</i> _a (mV)	<i>B</i> _c (mV)	<i>E</i> _{corr} (V)	<i>i</i> _{corr} μA/cm ²	<i>IE</i> %	<i>R</i> _{ct} Ohm	<i>C</i> _{dl} (μF/cm ²)	<i>IE</i> %
Blank	147.00	141.00	-0.4034	745	_____	1.80	334	_____
50 ppm	72.95	95.34	-0.4340	195	73.82	7	185	74.28
150	99.50	107.58	-0.4626	157	78.92	8.6	139	79.06
250	86.23	104.01	-0.4674	71	90.46	20	113	91.00

It is shown that, the i_{corr} decreased with increasing the inhibitor concentration. The curves of anodic and cathodic currents were changed with increasing concentrations of inhibitor. This implies that, Myrrh and magnetite/Myrrh Nanocomposite act as mixed inhibitors. The protection efficiency (PE%) is evaluated from i_{corr} values using the relationship [30-31]:

$$\text{PE\%} = 1 - i_{\text{corr}}(\text{inh}) / i_{\text{corr}}^0 \times 100 \tag{1}$$

where $i_{\text{corr}}(\text{inh})$ and i_{corr}^0 are corrosion current densities in the presence and absence of inhibitor, respectively. The values of PE% with different inhibitor concentrations for Myrrh and magnetite Myrrh Nanocomposite are listed in Table 1, and 2, respectively. The protection efficiency values in the Table 1 and 2 showed that the Myrrh and magnetite Myrrh nanocomposite act as very effective corrosion inhibitors for steel in HCl solution and their capacity of inhibition increased with increase of concentration. In addition, the employed concentrations of inhibitor were very small indicating that the effectiveness of the Myrrh and magnetite Myrrh Nanocomposite as good corrosion inhibitors for steel in 1M HCl solution. The higher value of the PE% in Magnetite Myrrh Nanocomposite than in Myrrh alone can be attributed to the synergistic effect of Magnetite nanoparticles, which enhances the adsorption of more inhibitors on steel surface and increase the PE%.

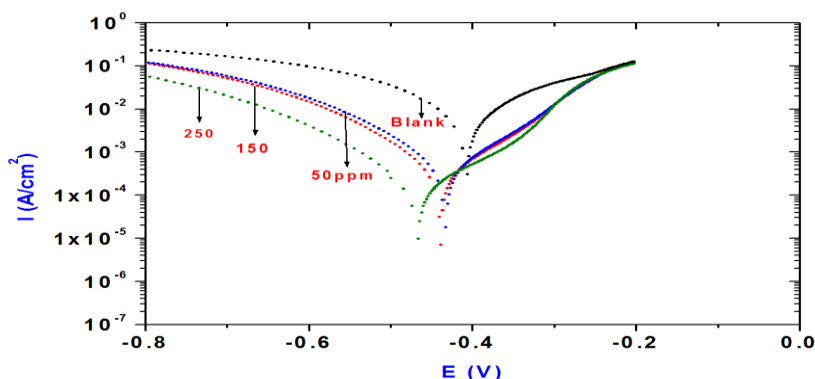


Figure 5. Polarization curves for steel in 1M HCl solution containing Myrrh with different concentrations.

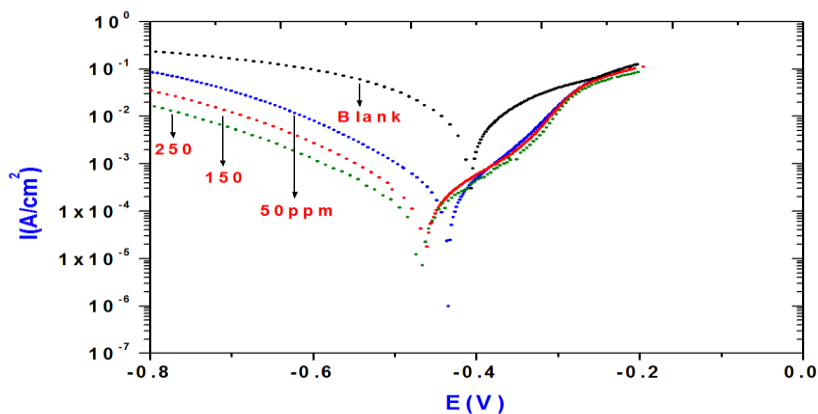


Figure 6. Polarization curves for steel in 1M HCl solution containing magnetite / Myrrh nanocomposites with different concentrations.

3.3 EIS measurement

Impedance spectra for steel in M HCl solution, in the absence and presence of various concentrations of Myrrh and magnetite/ Myrrh Nanocomposite are shown in Figures 7 and 8, respectively. The semicircle in all cases corresponds to a capacitive loop and the diameter of the capacitive loop increases with increasing concentration in both solutions. The results of EIS data indicated that the corrosion of steel in 1M HCl is controlled by a charge transfer process. The equivalent circuit employed for fitting the experimental data composed of a parallel combination of the charge transfer resistance (Rct) and the double layer capacitance (Cdl), both in series with the solution resistance (Rs). The impedance parameters for Myrrh and magnetite/ Myrrh Nanocomposite obtained by fitting the EIS data to the equivalent circuit are listed in Table 1 and 2, respectively. It should be noted from Table 1 and 2 that whilst charge transfer resistance values increase with increasing additive concentration, the capacitance values decrease indicating the formation of a surface protective film on steel surface. The high Rct values, are generally associated with slower corroding system [32-33]. The decrease in the Cdl can be attributed to a decrease in the local dielectric constant and/or from the increase of thickness of the electrical double layer [34]. Thus, the decrease in Cdl values and the increase in Rct values can be accounted to gradual replacement of water molecules by the adsorption of the inhibitor molecules on the steel surface. The protection efficiency (PE%) was calculated from the charge transfer resistance (Rct) using the following formula:

$$PE\% = 1 - R_{1ct}/R_{2ct} \times 100 \tag{2}$$

where R_{1ct} and R_{2ct} are the charge transfer resistances in absence and presence of the inhibitors, respectively. The values of PE% at different inhibitor concentrations are given in Table 1 and 2 for Myrrh and Magnetite Myrrh Nanocomposite, respectively. The higher value of PE% with the addition of magnetite nanocomposite to Myrrh can be attributed to a rapid increase in the adsorption of the inhibitor with a formation of film uniformity on steel surface. This can be explained by large interaction of the inhibitor molecule with the steel surface in the presence of Magnetite Nanocomposite, so that the steel surface is entirely and homogenously covered with protective surface film. It can be concluded that the protection efficiency calculated from polarization curves, and electrochemical impedance spectroscopy measurements are in good agreement.

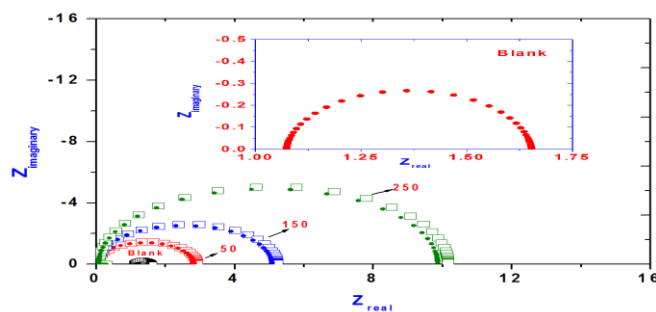


Figure 7. Nyquist diagram for steel in 1 M HCl solution containing Myrrh with different concentrations showing experimental (square) and fitted data (circle).

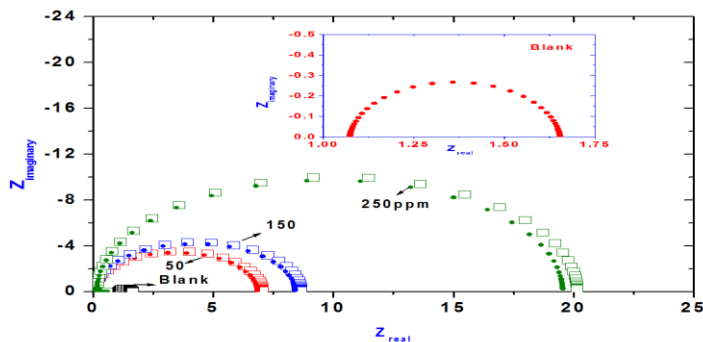


Figure 8. Nyquist diagram for steel in 1 M HCl solution containing Myrrh + magnetite nanoparticles with different concentrations showing experimental (square) and fitted data (circle).

4. CONCLUSIONS

1. Highly dispersed magnetite/Myrrh nanocomposites having monodisperse particles size were prepared using cheap capping agent .
2. The investigated Myrrh and magnetite/Myrrh nanocomposites exhibit inhibiting properties for corrosion of steel in 1 M HCl.
3. Myrrh and magnetite/Myrrh nanocomposites inhibit both anodic and cathodic reactions by adsorption on the steel surface and hence behaved like mixed type inhibitors.
4. Corrosion inhibition efficiencies of Myrrh and magnetite/Myrrh nanocomposites increased with their concentration and their values obtained from polarization and EIS methods are in good agreement.
5. The data concluded that the magnetite Myrrh Nanocomposite can be used as corrosion inhibitor for steel in 1 M HCl.

ACKNOWLEDGMENTS

This project was supported by King Saud University, Deanship of Scientific Research, Research Chair.

References

1. G. Gece, *Corros. Sci.*, 53 (2011) 3873–3898..
2. A.A. Rahim, E. Rocca, J. Steinmetz, M.J. Kassim, R. Adnan, M. Sani Ibrahim, *Corros. Sci.*, 49 (2007) 402–417.
3. P.B. Raja, M.G. Sethuraman, *Mater. Lett.*, 62 (2008) 113–116.
4. H. Bentrah, Y. Rahali, A. Chala, *Corros. Sci.* 82 (2014) 426–431.
5. M.A. Abu-Dalo, A.A. Othman, N.A.F. Al-Rawashdeh, *Int. J. Electrochem. Sci.* 7 (2012) 9303–9324.
6. E.E. Oguzie, Y. Li and F.H. Wang, *J. Colloid & Interface Sci.* 310 (2007) 90–98.
7. P.C. Okafor, M.E. Ikpi, I.E. Uwah, E.E. Ebenso, U.J. Ekpea, S.A. Umoren, *Corrosion Science* 50 (2008) 2310–2317.
8. K. Srivatsava, P. Srivatsava, *Br. Corros. J.*, 16 (1981) 221.

9. S.A Umoren, I.B. Obot, E.E Ebenso, P.C. Okafor, O. Ogbobe, E.E. Oguzie, *AntiCorros. Meth. Mat.*, 53(5) (2006) 277–282.
10. R.R. Baker, J.G. Mather, J.H. Kennaugh, *Nature* 301 (1983) 79.
11. K.V. Basavaiah, A.Prasada Rao, *Current Nanoscience* 8 (2012) 215-220.
12. L.C. Fidale, M. Nikolajski, T. Rudolph, S. Dutz, F.H. Schacher, T. Heinze, *J Colloid Interface Sci* 390 (2013) 25–33.
13. C. Jingting, L. Huining, Z. Yi, *Int J Nanomedicine* 6 (2011) 285–294.
14. Y.H. Deng, C.C. Wang, J. H. Hu, W. L. Yang, S. K. Fu, *Coll Surf A: Physicochem Eng Aspects*, 262 (2005) 87-93.
15. M. Das, P. Dhak, S. Gupta, D. Mishra, T.K. Maiti, A. Basak, P. Pramanik, *Nanotechnology*, 21 (2010) 125103-125109.
16. W. Wu, Q. He, C. Jiang, *Nanoscale Res. Lett.*, 3 (2008) 397-415.
17. T. Fried, G. Shemer, G. Markovich, *Adv. Mater.*, 13 (2001) 1158-1161.
18. S.J. Park, S. Kim, S. Lee, Z.G. Khim, K. Char, T. Hyeon, *J. Am. Chem. Soc.*, 122 (2000) 8581-8582.
19. J. Park, K. An, Y. Hwang, J.G. Park, H.J. Noh, J.Y. Kim, J.H. Park, N.M. Hwang, T. Hyeon, *Nat. Mater.*, 3 (2004) 891-895.
20. A.M. Atta, H.A. Al-Lohedan, S.A. Al-Hussain, *Molecules*, 19 (2014)11263-11278.
21. A. M. Atta, G. A. EL-mahdy, H. A. AL-Lohedan, *Digest Journal of Nanomaterials and Biostructures*, 9 (2014) 627-639.
22. G.A. El-Mahdy, A.M. Atta, H.A. Al-Lohedan, *Molecules*, 19 (2014) 1713-1731.
23. G.A. El Mahdy, A.M. Atta, A.K. F. Dyab, H.A. Al-Lohedan, *Journal of Chemistry*, 2013 (2013), Article ID 125731, 9 pages.
24. A. M. Atta, O. E. El-Azabawy, H.S. Ismail, *Corrosion Sci.*, 53 (2011) 1680–1689.
25. B. T. Amid, H. Mirhosseini, S. Kostadinović, *Chemistry Central Journal*, 6 (2012)117-129.
26. Nagata, T.; Fukushi, K. *Geochim. Cosmochim. Acta*, 74 (2010) 6000–6013.
27. A.. Atta, H. Al-Shafey, *Int. J. Electrochem. Sci.*, 8 (2013) 4970 – 4985.
28. A. M. Atta, G.A. El-Mahdy, H.A. Al-Lohedan, A. O. Ezzat, *Molecules*, 19 (2014) 10410-10426.
29. G. A. El-Mahdy, A.M. Atta, H.A. Al-Lohedan, *Molecules*, 19 (2014) 1713-1731.
30. E. McCafferty, *Corros. Sci.* 47 (2005) 3202.
31. Q. Qu, L. Li, W. Bai, S. Jiang, Z. Ding, *Corros. Sci.* 51 (2009) 2423.
32. K.F. Khaled, *Electrochim. Acta* 48 (2003) 2493.
33. K. Babic-Samardzija, C. Lupu, N. Hackerman, A.R. Barron *Langmuir* 21 (2005) 12187.
34. E. McCafferty, N. Hackerman, *J. Electrochem. Soc.* 119 (1972) 146.